The role of new zinc incorporated monetite cements on osteogenic differentiation of human mesenchymal stem cells

G. Cama [a,b,*], S. Nkhwa [a], B. Gharibi [a], A. Lagazzo [c], R. Cabella [d], C. Carbone [d], P. Dubruel [b], H. Haugen [e], L. Di Silvio [a], S. Deb [a]

[a]Tissue Engineering & Biophotonics Division,King's College London, Dental Institute, Floor 17, Tower Wing, Guy's Hospital, London, UK

[b]Polymer Chemistry & Biomaterials Group, Ghent University, Krijgslaan 281 (S4-bis), B-9000, Ghent, Belgium

[c]Department of Civil, Chemical and Environmental Engineering (DICCA), University of Genoa, P.le Kennedy 1, 16129 Genoa, Italy

[d]Dipartimento di Scienze della Terra, ell'Ambiente e dellaVita (DISTAV), University of Genoa, Corso Europa 26, 16132 Genoa, Italy

[e]University of Oslo, Department of Biomaterials, Institute for Clinical Dentistry, POBox 1109. Blindern, Oslo, NO0317, Norway

doi: https://doi.org/10.1016/j.msec.2017.04.086

Pubblicato su
"Materials Science and Engineering C 78 (2017) 485–494

Accettato 15 April 2017

Highlights

The fabrication of novel zinc incorporated monetite cements is reported
The setting reaction of the cements was carried out in presence of β-TCP reagent powders doped with zinc ions
The release of zinc from the monetite cement regulated the late response of hMSCs

Keywords
Monetite cement, Zinc, Human mesenchymal stem cells, Zinc doped β-tricalcium phosphate particles

Abstract

β-Tricalcium phosphate particles were sintered in the presence of different amounts (0–0.72 mol) of zinc oxide (ZnO) to prepare zinc doped β-TCP (Znβ-TCP) particles for further use in novel monetite (DCPA: CaHPO4) zinc incorporated bone cements with osteogenic differentiation potential towards human mesenchymal stem cells (hMSCs). XRD analysis of zinc incorporated cements prepared with β-TCP reagent particles doped with different amount of ZnO (i.e. 0.03, 0.09 and 0.18 mol ZnO) revealed the presence of unreacted Znβ-TCP and monetite. Furthermore, it was shown that zinc ions preferentially occupied the β-TCP crystal lattice rather than the monetite one. Release experiments indicated a burst release of ions from the different fabricated cements during the first 24 h of immersion with zinc concentrations ranging between 85 and 100% of the total concentration released over a period of 21 days. Cell proliferation significantly increased ($P<0.05$) on zinc incorporated monetite respect to control samples (Zinc-free cement) at 7 and 14 days post seeding. The expression of Runx-2 was significantly up regulated ($P<0.05$) in the case of cells seeded on monetite prepared with β-TCP doped with 0.03 moles of ZnO. On the other hand, the cell mineralization as well as the expression of osteogenic marker genes ALP and OSC decreased significantly ($P<0.05$) at 14 days post cell seeding. In conclusion, these results suggest that the zinc ions released from the cements during the first 24 h of culture played a critical role in regulating the osteogenic differentiation of hMSCs.

1. Introduction

Autologous bone transplantation continues to remain the gold stan- dard for treatment of bone loss due to different causes including osteo- myelitis, impact fractures due to trauma and those resulting from bone weakened by osteoporosis. The advantage of autologous over synthetic bone graft materials resides in its osteogenic and osteoinductive proper- ties [1]. However, bone is harvested generally from the patient's iliac crest and, as a consequence, requires a second operation at the site of tissue harvesting, which in turn may result in donor site injury and mor- bidity [2]. Furthermore, due to the limited amount of bone that can be harvested, autologous bone transplantation is not feasible for repairing large bone defects [3]. Therefore, a wide range of synthetic materials have been developed to overcome these drawbacks [4]. Among the dif- ferent types, calcium phosphate grafts are considered the most favoured
alternative to autologous bone grafts due to their osteoconductive properties and ability to osseointegrate [5,6]. Calcium phosphates based materials can be used in bone defects in the form of granules, solid blocks or injectable cements. The latter are obtained by mixing a calcium phosphate powder (in a single composition or a mixture) with a liquid phase and during the mixing of the cement, reagent dissolution and re-precipitation takes place forming a CaP cement paste that solidifies in a set time, which is dependent on the chemical formulation [7]. Once implanted, a bone graft should allow cellular ingrowth, whilst resorbing for newly formed tissue and support new

bone formation. Zinc ions have been shown to promote and sustain bone formation both in vitro and in vivo [8–10]. Hence, various studies have focused on the incorporation of zinc in the crystal lattice of bioceramics during high temperature synthesis or during the setting reaction of brushite cements [8, 11–15]. However, once implanted in the body, brushite tends to precipitate as insoluble hydroxyapatite (HA), slowing its replacement by bone [16]. On the other hand, anhydrous dicalcium phosphate (DCPA or monetite) is less soluble and appears not to transform to HA. Monetite is osteoconductive and resorbable in vivo [17,18], thus it forms an alternative to autologous bone grafts due to their osteoconductive properties and ability to osseointegrate [5,6]. Calcium phosphates based materials can be used in bone defects in the form of granules, solid blocks or injectable cements. The latter are obtained by mixing a calcium phosphate powder (in a single composition or a mixture) with a liquid phase and during the mixing of the cement, reagent dissolution and re-precipitation takes place forming a CaP cement paste that solidifies in a set time, which is dependent on the chemical formulation [7]. Once implanted, a bone graft should allow cellular ingrowth, whilst resorbing for newly formed tissue and support new bone formation. Zinc ions have been shown to promote and sustain bone formation both in vitro and in vivo [8–10]. Hence, various studies have focused on the incorporation of zinc in the crystal lattice of bioceramics during high temperature synthesis or during the setting reaction of brushite cements [8, 11–15]. However, once implanted in the body, brushite tends to precipitate as insoluble hydroxyapatite (HA), slowing its replacement by bone [16]. On the other hand, anhydrous dicalcium phosphate (DCPA or monetite) is less soluble and appears not to transform to HA. Monetite is osteoconductive and resorbable in vivo [17,18], thus it forms an excellent candidate as a bone repair material or as a matrix for bone tissue engineering.

Earlier we reported a novel straightforward method for the production of porous monetite cements [19] and the same procedure was adopted to form zinc incorporated monetite cements in this study. The preparation of the cements was carried out in two steps:

1. Sintering of Zn-doped β-TCP (Znβ-TCP) particles in the presence of different amounts (0–0.72 mol) of zinc oxide (ZnO).
2. Mixingofthehomemadeβ-TCPorZnβ-TCPwithcommerciallyavailable monocalcium phosphate monohydrate (MCPM) particles in the presence of a liquid phase.

The dissolved zinc from the lattice of the doped Znβ-TCP during the setting is expected to enter within the monetite crystals, whilst unreacted Znβ-TCP particles in the set cement are expected to act as carrier of Zn ions in liquid medium. The Znβ-TCP particles were formed using a range of concentrations of zinc oxide. Amounts lower or equal to 0.09 mol yielded β-TCP particles with the zinc ions within the lattice. However, higher concentrations (from 0.18 up to 0.72 mol) led to the formation of a mixture of unreacted ZnO, Znβ-TCP and a zinc calcium phosphate phase ($ZnCa_2(PO_4)_2$). The aim of this work was the investigation of how the zinc changes the molecular microstructure of the phosphate cement and as the presence of Zinc in the dissolution medium of the phosphate has an influence on the cell biological response. Hence we investigated for the first time the proliferation and differentiation of hMSCs seeded on zinc incorporated resorbable monetite.

2. Experimental

2.1. β-TCP and Zn-doped β-TCP (Znβ-TCP) powders synthesis

β-TCP and Zn-doped β-TCP (Znβ-TCP) powders were prepared by a solid state reaction as shown in Eq. (1). Briefly, β-TCP powders doped with a molar percentage of Zn^{2+} ions ranging between 0 and 24% per mole of Ca^{2+} ions present in the β-TCP lattice were obtained by mixing zinc oxide, (ZnO, Sigma Aldrich, assay ≥99%) calcium phosphate dibasic ($CaHPO_4$, Sigma Aldrich, assay N98%) and calcium carbonate ($CaCO_3$, Sigma Aldrich, assay ≥99%) powders in a mortar for 5 min. Then, the whole mass was transferred to a steel mould and subjected to a pressure of 1 MPa for 2 min in order to obtain pellets with a volume of ca. 0.34 cm^3. The resulting pellets were

calcined in a furnace at a temperature of 1000 °C for 12 h in air. The different sintered powders were labelled in reference to the molar percentage of ZnO used (Table 1).

$$2CaHPO_4 + (1-x)\,CaCO_3 + xZnO = Ca_{(3-x)}\,Zn_x\,(PO_4)_2 + H_2O + (1-x)CO_2 \quad (1)$$

x = moles of Zn introduced in the powder mixture.

2.2. Monetite cement preparation, setting time and SEM analysis

Monetite cements were prepared following the method described by Cama et al. [19] with the modifications, in which the cement precursors were Znβ-TCP particles. The setting times of the cements (n = 3) were evaluated using the Gilmore test according to ASTM C266-99 standard. The morphology of the sintered β-TCP powders and the microstructure of the monetite cements were observed by scanning electron microscopy (SEM-EDX, a Hitachi S-3500, Tokyo, Japan).

2.3. FTIR/ATR spectroscopy and X-ray powder diffractometry

FTIR/ATR measurements were performed by using a FT instrument (Perkin Elmer Spectrum One FT-IR Spectrometer, PerkinElmer Instrument, USA) with a resolution of 4 cm^{-1}. The crystalline compounds within the samples were determined using X-ray powder diffractometry (XRPD, PANalytical Corporation, Netherlands) with CoKα radiation. Samples were ground with an agate mortar and pestle, and the dry powders were mounted on zero-background silicon plates. Each sample was scanned between 3 and 70° 2θ at a scan rate of 1° per minute. Identification was done using X' Pert High Score software (X'Pert-Pro MPD, Philips, Eindhoven, PanaLytical Corporation Netherlands) by comparing the diffraction pattern of the unknown compound against patterns for known compounds listed in the Powder Diffraction File (PDF 2000) database.

2.4. Diametral compressive strength and micro-CT analysis

The diametral strength of disc shaped specimens (n = 12, d = 8.4 mm, h = 4.2 mm) tested in compression was determined using a universal testing machine (Instron 5569A, Instron Corporation, USA) with a load cell of 500 N and a crosshead rate of 1 mm/min. The specimens after 24 h from the setting reaction were soaked for 24 h in distilled water and then still wet immediately tested. The porosity of the monetite cements were assessed using micro-CT imaging (SkyScan 1172 high-resolution micro-CT, Bruker micro-CT, Kontich, Belgium). All samples were scanned both at 4.96 µm voxel resolutions using a source voltage of 100 kV and a current of 100 µA with 0.5 mm aluminium filter to optimise the contrast. Samples were rotated 360° around their long axis and four absorption images were recorded every 0.400° of rotation. These raw images were then reconstructed with the standard Bruker micro-CT reconstruction software (NRecon, Version: 1.6.9.3, Bruker micro-CT., Kontich, Belgium) to serial coronal-oriented tomograms using 3D cone beam reconstruction algorithm. For reconstruction, beam hardening was set to 25% and ring artefact reduction to 12. The image analysis of the reconstructed axial bitmap images was performed using standard Bruker micro-CT software (CTan and CTvox). Cylindrical volume of interest (VOI) with a diameter of 4.0 mm and height of 3.5 mm was defined in the middle of each material. The greyscale threshold of binarised images was set from 50 to 255. Additional noise was removed by ‘despeckling’ function which removed all objects smaller than 1200 voxels that were not connected to the 3D object prior to further analysis and filtered with a Gaussian blur radius 2.0. The key 2D and 3D pore architecture parameters for each material both were then calculated in the CTan software. The 3D images were done in CTVox.

2.5. Calorimetry and ion release studies

A Calvet-type calorimeter (Setaram C80, SETARAM Instrumentation, Caluire, France) was used to measure the enthalpy of dissolution in water of ZnO and β-TCP powders obtained these latter by sintering in presence of 0, 3 and 6% ZnO, with a powder-liquid ratio P/L = 2:1. The heat changes during the setting of the cements prepared by using β-TCP with 0, 3 and 6% ZnO respectively were also determined as previously described [19] and measurements were conducted at 37 °C. The ions release study was carried out using three samples (d = 8.4 mm, h = 4.2 mm) for each type of cements (i.e. cement 0, 1, 3 and 6% ZnO). The samples were sterilised by gamma irradiation at a dose of 31.8 kGy and were immersed for 1, 3, 7, 14 and 21 days into 3 ml of double distilled water (Sigma Aldrich) at 37 °C. At each time point, the samples were replaced in fresh water and the eluents collected. The measurements were performed by inductively coupled plasma (ICP) spectroscopy (Thermo iCAP 6000 ICP emission spectrometer, Thermo Electron Corporation, USA).

2.6. In vitro cell culture

Human primary mesenchymal stem cells (hMSC) was purchased from Lonza (Slough, UK) and cultured in α-Minimal Essential Medium (MEM), penicillin (50 U/ml), streptomycin (50 μg/ml) (all from Sigma–Aldrich, Poole, Dorset, UK), Glutamax (2 mM) (Invitrogen, Paisley, UK), 10% fetal bovine serum (FBS) (Sigma– Aldrich) added and maintained at 37 °C in a humidified 5% CO_2: 95% air atmosphere.

2.7. Cell proliferation: Alamar Blue assay

The monetite cements were sterilised by gamma irradiation at a dose of 31.8 kGy. Cell proliferation was determined using the AlamarBlueTM assay (Life technologies) which is a redox indicator that measures proliferation quantitatively. Cells were micro seeded at a total density of 1×10^5 cell per cement (d = 8.4 mm, h = 4.2 mm) placed in a 24 well plate. The time period studied were 1, 3, 7, 14 and 21 days. The cell culture media was changed after 24 h and every 3 days subsequently.

2.8. Quantitative RT-PCR analyses and mineralization

To assess osteogenic differentiation, cells were either micro seeded on the cements or tissue culture plastic plates. Osteogenesis was induced with growth medium supplemented with 0.1 μM dexamethasone, 0.05 mM ascorbic acid and 10 mM glycerophosphate (Sigma–Aldrich). mRNA expression, the markers of differentiation (i.e. Runx-2, ALP and OSC) was determined on cells directly seeded on the cements by quantitative (q)RT-PCR. Total RNA was extracted using TRI reagent (Ambion, Warrington, UK) according to the manufacturer's instructions. RNA purity and quantity was assessed by nanodrop (Thermo Fisher Scientific, Waltham, USA), and cDNA prepared using QuantiTect Reverse Transcription Kit (Qiagen, West Sussex, UK) according to the manufacturer's instructions. qRT-PCR was performed on a Mx3000P real time PCR system (Stratagene, Agilent Technologies, Cheshire, UK) using iTaq SYBR Green qPCR master mix (Bio-Rad) and the following primer pairs: (5′ to 3′) RPL13a (GGATGGTGGTTCCTGCTG and TGGTACTTCCAGCCAACCTC); Runx-2 (AATGGTTAATCTCCGCAGGTC and TTCAGATAGAACTTGTAC CCTCTGTT); ALP (AACACCACCCAGGGGAAC and TGGCATGGTTCACTCT CGT) and osteopontin (GCCGAGGTGATAGTGTGGTT and TGAGGTGATGT CCTCGTCTG). PCR conditions consisted of 1 cycle at 95 °C for 40 s and 40 cycles at 95 °C for 5 s and 60 °C for 10 s followed by melting analysis of 1 cycle with gradual increase from 65 °C to 95 °C. RPL13a was used as an invariant housekeeping gene. Changes in mineralization was visualised on cells seeded on tissue culture plates in presence or absence of cements by staining with Alizarin Red dye. In brief, cells were washed with PBS, fixed (4%

formaldehyde in PBS) for 15 min, washed with distilled water, stained for 10 min, washed in 50% ethanol and air dried.

2.9. Data analysis

Statistical comparisons between means were made by Student's ttest (SPSS 16, SPSS Inc., Chicago, USA). A P-value of b0.05 was considered statistically significant.

3. Results and discussion

3.1. Characterization of the sintered β-TCP powders

Different amounts of ZnO powders were added to a mixture of DCPA and $CaCO_3$ (Eq. (1)) and eight different Zn doped β-TCP particles (Table 1) were prepared and analysed by XRPD. XRPD analysis was also performed on commercial β-TCP (Sigma-Aldrich, assay N 96) which was used as reference together with the patterns for known compounds listed in the Powder Diffraction File (PDF 2000) database. The XRPD pattern reported in Fig. 1A revealed the peaks associated with β-TCP however the commercial sample of β-TCP, showed the presence of trace amounts of an unknown substance which may be ascribed to β-calcium pyrophosphate (β-CPP). These results are in agreement with the FTIR measurements shown in Fig. 2, where the characteristic vibration mode of PO_4 tetrahedra is the predominant peak indicative of a crystalline β-TCP phase for both sintered and commercial powders. The small absorption peaks at 728 cm^{-1} and 1211 cm^{-1} detected for commercial β-TCP are attributed to the vibration mode of the pyrophosphate groups ($P_2O_7^{4-}$) [20]. The XRPD results of the samples prepared with different amount of ZnO also showed appreciable peak shifts and variations of peak intensities related to Zn in the β-TCP structure (Fig. 1B). The XRD patterns of Znβ-TCP produced with percentages of ZnO ≤ 3 (i.e. x ≤ 0.09 mol), showed the presence of β-TCP or Znβ-TCP as unique phases present in the powders (Fig. 1B). This result is in perfect agreement with the data reported in literature by Kawabata et al. [11] which showed that β-TCP powder synthesised in presence of different Zn concentration (x = 0, 0.01, 0.03, 0.05 and 0.1 in $Ca_{3-x}Zn_x(PO_4)_2$) were single-phased β-TCP and that there were no precipitates in the sample specimens due to Zn-doping. On the other hand, the XRPD patterns for higher ZnO amounts ranging between 6 and 24% suggest the existence of a hybrid solid solution $Ca_3(PO_4)_2$ - $ZnCa_2(PO_4)_2$. The peak intensities show an increase of ZnO in the samples and the XRPD patterns obtained for the highest amount of ZnO used and equal to 24% indicated the formation of a Zn calcium phosphate phase ($ZnCa_2(PO_4)_2$) (Fig. 1C). The substitution of Ca^{2+} with Zn^{2+} ions is further testified by the decrease of both the unit cell parameters and the cell volume of β-TCP (Fig. 3). Both decreases are due to the Zn ions occupying the crystal lattice, which have a lower ionic radius (0.74 Å) with respect to that of calcium (0.99 Å) [21]. The FTIR spectra of powders obtained in presence of percentages of ZnO ≥ 6 changed with respect to the one measured on control powders (0% ZnO) (Fig. 4). The characteristic stretching peaks (ν-PO) of the PO group (968 and 943 cm^{-1}) broadened due to a decrease in crystallinity with higher concentrations of Zn [22], a new peak at 927 cm^{-1} appeared in the spectra of samples sintered with 6 and 12% moles of ZnO. Furthermore, the stretching modes of the PO group at 1036 and 1018 cm^{-1} merge in a single peak at 1005 cm^{-1} and in the case of samples sintered in the presence of 24% moles of ZnO, two new peaks were observed at 952 and 1164 cm^{-1}, which may be attributed to the Zn calcium phosphate phase detected by XRD measurements.

3.2. XRPD analysis of monetite cements

The XRPD pattern of the control cement (0% ZnO) confirmed the presence of monetite and unreacted β-TCP (Fig. 1C). The intensity and number of the diffraction peaks ascribed to the β-TCP phases (β-TCP and ZnβTCP) increased, although not quantified, with the increasing amount of ZnO used during sintering (Fig. 1D). Moreover, the displacement of peak positions of the Zn (see inset Fig. 1D) is evidence of the Zn ions entering preferentially in β-TCP structure rather than in those of monetite. In order to investigate the reason behind the increase of unreacted β-TCP in the set cements, we measured by calorimetric analysis the heat of dissolution of β-TCP in water. A dramatic increase, in absolute value of the enthalpy of dissolution, from −0.1 J/g for β-TCP to − 1.06 J/g and − 1.03 J/g for β-TCP sintered with 3% and 6% ZnO respectively (Table 2) suggests a reduction in the stability of the lattice, probably due to the changes of the elementary cell dimensions (Fig. 3) producing internal stresses. Furthermore, because the enthalpy of dissolution of ZnO is lower than those measured for the Zn doped β-TCP powders, we can attribute the increase of enthalpy due to the introduction of Zn in the crystal lattice. Surprisingly, despite the increase in the solubility of the Znβ-TCP particles, the setting time of cements (cement 6% ZnO, final setting time N 24 h) increased with respect to that of control samples (cement 0% ZnO, final setting time = 45 ± 1 min). The setting time measurements suggested a decrease of the exothermic dissolution rates of the Znβ-TCP particles. In order to validate this finding, we studied the kinetic of reaction of the cements prepared by mixing equimolar amount of MCPM and the in house prepared β-TCP particles in distilled water. As anticipated, the formation of brushite occurred [19]. The heat flow generated during the setting reaction decreased from 30.9 mW to 4.6 mW in the presence of Znβ-TCP particles (Table 3 and Fig. 5). The corresponding decrease of the enthalpy of reaction from − 54.4 kJ/mol to − 31.6 kJ/mol and − 19.2 kJ/mol in the presence of Znβ-TCP particles (sintered in the presence of 3 and 6% ZnO respectively) can be explained with a complex phenomenon comprehensive of a lower degree of advancement of the reaction, with the partial formation of monetite (−11 kJ/mol against −83 kJ/mol in the case of brushite formation) [23]. Furthermore, the presence of monetite in brushite cements prepared with Znβ-TCP particles was detected by FTIR measurements (Fig. 6), which showed the reduction of the peak intensities at 1203 and 775 cm^{-1} associated with the bending and vibration modes of the O\\H bond respectively, arising from the water of crystallization in brushite as well as the appearance of the typical P– OH bending mode of monetite at 1404–1353 cm^{-1} [24]. Taken together, these results suggest that the presence of unreacted TCP cannot be ascribed to a decrease of particle solubility due to the Zn substitution. Further evaluations are needed in order to elucidate this phenomenon.

3.3. Morphological analysis of the powders and cements

The scanning electron micrographs of the β-TCP particles prepared in house with and without inclusion of zinc are shown in Fig. 7. The morphology of the control β-TCP particles (0% ZnO) and those prepared with molar amounts of ZnO lower than 9% appeared as globular particles with rounded edges accompanied with an increase in the size of the particle agglomerates due to the presence of ZnO during sintering. However, with 9% of zinc oxide in the feed mixture, there is evidence of the particles becoming flatter and irregular and this trend was more pronounced with increasing concentration of zinc oxide as a result of the fusion of the particle aggregates (Fig. 7G–H). Furthermore, the porosity was drastically reduced due to densification (Fig. 7G–H). The series of micrographs at the same magnification clearly indicates that the amount of ZnO in the mix had a bearing on the size of the sintered β-TCP particles and revealed its effectiveness as dopant that is able to alter the grain boundary regions of the fabricated TCP particles.

The scanning electron micrographs of monetite prepared with both control and zinc doped (%ZnO ≤ 3) particles showed the formation of a similar cement microstructure characterised by platelet-like crystals of similar size (data not shown). On the other hand, the microstructure of the cements prepared with β-TCP particles doped with 6% ZnO showed the formation of monetite crystals with

larger size (Fig. 8B) and the particles seem to coalesce. The increase of the crystal size may be ascribed to the higher setting time for this cement which, in turn, may enhance the formation of more bulky crystals with a lamellar surface structure as shown in Fig. 8A. Moreover, as reported by the XRD patterns, unreacted TCP was detected in the different types of prepared cements (Fig. 8A and B).

3.4. Micro-CT and tensile testing

Micro-CT analysis showed that the total porosity of the cements ranged between 25 and 29% (Table 4). The diametral tensile strength was about 50% lower ($P<0.05$) for the cement 6% ZnO, despite a porosity very similar (the total porosity of the cements was 29% and 22% for the cement 0% and 6% ZnO respectively) to the control monetite cement (cement 0% ZnO). This may be attributed to the higher amount of unreacted precursor particles in the cement matrix that may act as inclusions, producing stress concentration sites, due to the mismatch in elastic modulus with the monetite phase. Consequently, the ceramic inclusions may favour the nucleation and propagation of cracks lowering the mechanical strength of the cements.

3.5. Ions release and biological tests

The release of Ca, phosphate and Zn ions from the cements with 0, 1, 3 and 6% ZnO were determined at 1, 3, 7, 14 and 21 days and the immersion medium refreshed at each time point. A burst release of the ions were observed, in particular 100, 94 and 85% of the total Zn ions were released in the first 24 h from the sample fabricated with β-TCP doped with 0.03, 0.09 and 0.18 mol ZnO respectively when measured over 21 days. Instead, the amount of calcium and phosphate in the first 24 h were 56, 60, 60% and 60, 62, 66% of the total amount of the respective ions released over a period of 21 days (Tables 5-7). The decrease of the ions released with increasing immersion time may be due to the lack or poor refreshment of water within the cement pores, which in turn may bring about a kinetic equilibrium between the rates of ion dissolution and re-precipitation onto the pore walls.

In vitro cell culture studies using human mesenchymal stem cells showed that both monetite cements with and without Zn supported cell adhesion. Moreover, a prominent cytoplasmic extensions (Fig. 9B and C) was observed in the case of cells seeded on the cement 1 and 3% ZnO and this trend became more evident on the cement 6% ZnO with the cells tend to spread forming thin layers which covered almost entirely the sample surface (Fig. 9D). The enhancement on cell spreading onto the cement 6% ZnO can be ascribed at the greater amount of Zinc released during the first 3 days of culture (about 90 and 54% higher than that one measured for the cement 1 and 3% ZnO respectively). These results are in agreement with the study of Hu et al. [25] where the adhesion of bone marrow stem cells seeded onto Zn-incorporated TiO_2 coatings on titanium was found to be more pronounced with increasing Zn content in the coatings. A Zn concentration of about 0.138 mM was released during the first 24 h of immersion from the cement 1% ZnO which corresponded with significant increase in cell proliferation at 7 and 14 days in comparison to MSC seeded on Zn-free samples (Fig. 10). Increase in cell growth at 7 and 14 days also coincided with Zn concentrations ranging between 1.35 mM and 0.004 mM released over a period of 14 days (Fig. 10 and Table 5). On the other hand, the cell mineralization (Fig. 11) and the expression of ALP and OSC was lower ($P<0.05$) in comparison to those measured for cells seeded onto control samples (cement 0% ZnO, Fig. 12). Interestingly, the expression of Runx-2 was higher in cell cultured on monetite fabricated with β-TCP sintered in presence of 1% ZnO. Although our study was performed using water as the immersion medium, we expect a similar release rate in cell culture medium, because the amount of Zn released at 24 h from the cement fabricated with β- TCP sintered with 1% ZnO was also significantly higher ($P<0.05$) than the concentration value (0.1 mM) beyond which

the mineralization and osteogenic differentiation have been reported to be impaired [12, 26]. Hence on account of the decrease of ALP and OSC observed, we may expect that, at 24 h post cell seeding the amount of Zn released from the cements was comparable to this value and then the one measured in our study (0.138 mM). Moreover, because longer immersion time did not result in more Zn ions release, the Zn released during the first 24 h regulated the responses of hMSCs at longer culture time promoting proliferation and at the same time inhibiting osteogenic gene expression (7 and 14 days in the case of cell proliferation and 14 days in the case of gene expression). This observation is further supported by the fact that, after the immersion medium was refreshed, the Zn concentrations decreased and were below (~47 μM, cement 3%ZnO) or slightly higher (~0.17 mM, cement 6% ZnO) of 0.1 mM.

4 Conclusions

In this study for the first time the fabrication of monetite bone cements containing zinc ions is reported. XRD analysis showed that the presence of zinc in the lattice of β-TCP did not impair the precipitation of monetite during the setting reaction as well as zinc ions entered preferentially the β-TCP crystal lattice over the monetite counterpart. The release of zinc ions in the range of 0.004–1.35 mM was found to enhance the cells proliferation at 7 and 14 days post seeding with respect to control samples (cement 0% ZnO). The lower expression of ALP and OSC measured with respect to control samples may be due to the initial burst dissolution, which caused the release of zinc in a concentration higher than those reported to impair osteogenic differentiation of bone cells. The different biological responses observed in this work suggest that the concentration of zinc released during the first 24 h of immersion was determinant on regulating the late responses hMSCs, favouring cell growth and at the same time inhibiting osteogenic differentiation. Given the antimicrobial activity of zinc ions, the future work will assess the antimicrobial properties of the fabricated zinc modified monetite over pathogens associated with bone infection.

References

[1] M.R. Urist, Bone: formation by Autoinduction, Science 150 (1965) 893–899.

[2] J.C. Banwart, M.A. Asher, R.S. Hassanein, Iliac crest bone graft harvest donor site morbidity, a statistical evaluation, Spine 20 (1995) 1055–1060.

[3] C.J. Damien, J.R. Parsons, Bone graft and bone graft substitutes: a review of current technology and applications, J. Appl. Biomater. 2 (3) (1991) 187–208.

[4] E. García-Gareta, M.J. Coathup, G.W. Blunn, Osteoinduction of bone grafting materials for bone repair and regeneration, Bone 81 (2015) 112–121.

[5] P. Fray, J.L. Trouillet, N. Rouquet, E. Azimus, A. Autefage, Osseointegration of macroporous calcium phosphate ceramics having a different chemical composition, Biomaterials 14 (1993) 423–429.

[6] M.Bohner,F.Theiss,D.Apelt,W.Hirsiger,R.Houriet,G.Rizzoli,E.Gnos,C.Frei,J.A. Auer, B. von Rechenberg, Compositional changes of a dicalcium phosphate dihydrate cement after implantation in sheep, Biomaterials 24 (2003) 3463–3474.

[7] G. Cama, F. Barberis, R. Botter, P. Cirillo, M. Capurro, R. Quarto, S. Scaglione, E. Finocchio, V. Mussi, U. Valbusa, Preparation and properties of macroporous brushite bone cements, Acta Biomater. 5 (2009) 2161–2168.

[8] A. Ito, H. Kawamura, M. Otsuka, M. Ikeuchi, H. Ohgushi, K. Ishikawa, K. Onuma, N. Kanzaki, Y. Sogo, N. Ichinose, Zinc-releasing Calcium Phosphate for Stimulating Bone Formation, 22, 2002 21–25.

[9] J. Ovesen, J.S. Thomsen, G. Danscher, L. Mosekilde, The Positive Effects of Zinc on Skeletal Strength in Growing Rats, 29, 2001 565–570.

[10] Y. Qiao, Biomaterials stimulation of bone growth following zinc incorporation into biomaterials, Biomaterials 35 (2014) 6882–6897.

[11] K. Kawabata, T. Yamamoto, A. Kitada, Substitution mechanism of Zn ions in β-tricalcium phosphate, Phys. B Condens. Matter 406 (2011) 890–894.

[12] M.Yamaguchi,M.Goto,S.Uchiyama,T.Nakagawa,Effectofzincongeneexpression in osteoblastic MC3T3-E1 cells: enhancement of Runx2, OPG, and regucalcin mRNA expressions, Mol. Cell. Biochem. 312 (2008) 157–166.

[13] S.Pina,S.I.Vieira,P.Rego,P.M.Torres,O.A.daCruzeSilva,E.F.daCruzeSilva,J.M. Ferreira, Biological responses of brushite-forming Zn- and ZnSr- substituted betatricalcium phosphate bone cements, Eur. Cell. Mater. 20 (2010) 162–177.

[14] K.Paul,B.Y.Lee,C.Abueva,B.Kim,H.J.Choi,S.H.Bae,B.T.Lee,Invivoevaluationof injectable calcium phosphate cement composed of Zn- and Si-incorporated β- tricalcium phosphate and monocalcium phosphate monohydrate for a critical sized defect of the rabbit femoral condyle, J. Biomed. Mater. Res. Part B Appl. Biomater. Mendeley Data 105 (2015) 260–271, http://dx.doi.org/10.1002/jbm.b. 33537.

[15] S.Pina,S.I.Vieira,P.M.Torres,F.Goetz-Neunhoeffer,J.Neubauer,O.A.daCruzeSilva, E.F. da Cruz e Silva, J.M. Ferreira, In vitro performance assessment of new brushite- forming Zn- and ZnSr-substituted b-TCP bone cements, J. Biomed. Mater. Res. B Appl. Biomater. 94 (2010) 414–420.

[16] F. Tamimi, Z. Sheikh, J. Barralet, Dicalcium phosphate cements: Brushite and monetite, Acta Biomater. 8 (2012) 474–487.

[17] F. Tamimi, J. Torres, D. Bassett, J. Barralet, E.L. Cabarcos, Biomaterials resorption of monetite granules in alveolar bone defects in human patients, Biomaterials 31 (2010) 2762–2769.

[18] F.Tamimi,D.LeNihouannen,H.Eimar,Z.Sheikh,S.Komarova,J.Barralet,Theeffect of autoclaving on the physical and biological properties of dicalcium phosphate dihydrate bioceramics: brushite vs. monetite, Acta Biomater. 8 (2012) 3161–3169.

[19] G. Cama, B. Gharibi, M. Saif Sait, J.C. Knowles, A. Lagazzo, S. Romeed, L. Di Silvio, S. Deb, A novel method of forming micro- and macroporous monetite cements, J. Mater. Chem. B 1 (2013) 958–969.

[20] P.M.C. Torres, J.C.C. Abrantes, A. Kaushal, S. Pina, N. Döbelin, M. Bohner, J.M.F. Ferreira, Influence of Mg-doping, calcium pyrophosphate impurities and cooling rate on the allotropic α ↔ β-tricalcium phosphate phase transformations, J. Eur. Ceram. Soc. 36 (2016) 817–827.

[21] A. Bigi, E. Foresti, M. Gandolfi, M. Gazzano, N. Roveri, Isomorphous substitutions in b-tricalcium phosphate: the different effects of zinc and strontium, J. Inorg. Biochem. 66 (1997) 259–265.

[22] F. Miyaji, Y. Kono, Y. Suyama, Formation and structure of zinc-substituted calcium hydroxyapatite, Mater. Res. Bull. 40 (2005) 209–220.

[23] M. Bohner, U. Gbureck, Thermal reactions of brushite cements, J. Biomed. Mater. Res. B Appl. Biomater. 84B (2008) 375–385.

[24] J. Xu, I.S. Butler, D.F.R. Gilson, FT-Raman and high-pressure infrared spectroscopic studies of dicalcium phosphate dihydrate ($CaHPO_4 \cdot 2H_2O$) and anhydrous dicalcium phosphate ($CaHPO_4$), Spectrochim. Acta A Mol. Biomol. Spectrosc. 55 (1999) 2801–2809.

[25] H. Hu, W. Zhang, Y. Qiao, X. Jiang, X. Liu, C. Ding, Antibacterial activity and increased bone marrow stem cell functions of Zn-incorporated TiO_2 coatings on titanium, Acta Biomater. 8 (2012) 904–915.

[26] M. Ikeuchi, A. Ito, Y. Dohi, H. Ohgushi, H. Shimaoka, K. Yonemasu, T. Tateishi, Osteogenic differentiation of cultured rat and human bone marrow cells on the surface of zinc-releasing calcium phosphate ceramics, J. Biomed. Mater. Res. A 67 (2003) 1115–1122.

Table captions

Table 1. The feed content of ZnO in moles is shown with the weight percentages. (%ZnO = percentage of moles of ZnO added to the powder mixture per mole of calcium ions present in the β-TCP lattice. x = moles of zinc introduced in the powder mixture).

Table 2. Enthalpy of dissolution in water of the Zn-doped β-TCP and ZnO powders as determined by calorimetric analysis.

Table 3. Reaction Kinetics of brushite cements expressed in terms of the enthalpy of reaction, the maximum value of the exothermic peak and the time at which it is achieved. (P/L = 2).

Table 4. Diametral tensile strength (n = 6) and porosity of the cements prepared with β-TCP powders sintered with different amounts of ZnO (0–6%).

Table 5. Concentrations of calcium ions released from the fabricated monetite cements soaked for different time points (1–21 days) in double distilled water.

Table 6 . Concentrations of phosphate ions released from the fabricated monetite cements soaked for different time points (1–21 days) in double distilled water.

Table 7. Concentrations of zinc ions released from the fabricated monetite cements soaked for different time points (1–21 days) in double distilled water.

Figure captions

Fig. 1. XRPD spectra of A commercial β-TCP (Sigma Aldrich assay N 96%) and sintered β-TCP (0% ZnO) powders. B: β-TCP powders sintered in presence of different molar amounts of ZnO (0, 3, 6, 12 and 24%). C: Monetite cement fabricated with undoped β-TCP (0% ZnO) and D: monetite cements fabricated with β-TCP powders doped with different molar amounts of ZnO (1–6%).

Fig. 2. ATR/FTIR of commercial (Sigma Aldrich) and sintered β-TCP (0% ZnO) powders.

Fig. 3. Lattice constants (A and B) and cell volume (C) of the β-TCP powders sintered with different amounts of ZnO (0–24% ZnO).

Fig. 4. ATR/FTIR of the β-TCP powders sintered with 0–6% (A) and 0–24% ZnO (B).

Fig. 5. Comparison between the heat-flow of brushite cements made by mixing in distilled water equimolar amounts of MCPM and β-TCP particles (0–6% ZnO). (P/L = 2).

Fig. 6. FTIR spectra of cements formed inside the calorimeter device. The acquisition was performed after 30 min from the start of the mixing of equimolar amount of β-TCP (0% ZnO or 6% ZnO) and MCPM using distilled water as liquid phase with a P:L ratio of 2:1.

Fig. 7. Micrographs of β-TCP powders sintered in presence of different amounts of ZnO (1–24% ZnO).

Fig. 8. SEM images of monetite cements prepared with β-TCP powders sintered without (A: 0% ZnO) and with ZnO (B: 6% ZnO).

Fig. 9. SEM images (500×) of MSCs seeded on monetite cements made with βTCP particles (3 days post seeding) sintered with different amount of ZnO (0–6%).

Fig. 10. hMSCs proliferation on monetite cements prepared with β-TCP powders sintered with different amount of ZnO (0–6%). *P < 0.05 vs 0% ZnO (control cements).

Fig. 11. Optical photographs showing the mineral agglomerates (red stained regions reported in the pictures) produced by hMSCs which were seeded on the well plate (A) and put in contact with the external surface of cements fabricated with β-TCP particles sintered with 0 (B), 1 (C), 3 (D) and 6% (E) ZnO. The minerals' staining was performed at 14 days post cell seeding.

Fig. 12. hMSCs gene expression measured at 14 days post seeding on monetite cements fabricated with β-TCP particles sintered with different amount of ZnO (0–6%). *P < 0.05 vs control cements (0% ZnO).

.

ZnO %	ZnO Moles (X)	Powder	
0	0	$Ca_3(PO_4)_2$	→ β-TCP
1	0.03	$Ca_{2.97}Zn_{0.03}(PO_4)_2$	
3	0.09	$Ca_{2.91}Zn_{0.09}(PO_4)_2$	
6	0.18	$Ca_{2.82}Zn_{0.18}(PO_4)_2$	
9	0.27	$Ca_{2.73}Zn_{0.27}(PO_4)_2$	Znβ-TCP
12	0.36	$Ca_{2.64}Zn_{0.36}(PO_4)_2$	
18	0.54	$Ca_{2.46}Zn_{0.54}(PO_4)_2$	
24	0.72	$Ca_{2.28}Zn_{0.72}(PO_4)_2$	

Table 1

Powder	Enthalpy (J/g)
β-TCP 0% ZnO	−0.1
β-TCP 3% ZnO	−1.06
β-TCP 6% ZnO	−49.2
ZnO	−0.65

Table 2

Cement precursor powders	Enthalpy of reaction (kJ/mol)	Max exothermic peaks	
		Time (s)	Heat flow (mW)
β−TCP 0% ZnO + MCPM	−54	480	30.9
β-TCP 3% ZnO + MCPM	−31.6	660	9.3
β-TCP 6% ZnO + MCPM	−19.2	775	4.6

Table 3

Cement	σ_T (MPa) Mean ± SD	Total porosity %	Closed porosity %	Open porosity %
0% ZnO	1.31 ± 0.02	29	11	20
1% ZnO	1.50 ± 0.04	27	14	15
3% ZnO	1.25 ± 0.13	25	15	13
6% ZnO	0.72 ± 0.07	22	11	20

Table 4

day	Cement 0% ZnO Ca^{2+} (mM)	Cement 1% ZnO Ca^{2+} (mM)	Cement 3% ZnO Ca^{2+} (mM)	Cement 6% ZnO Ca^{2+} (mM)
1	3.20 ± 0.35	2.52 ± 0.24	2.69 ± 0.10	2.87 ± 0.29
3	0.83 ± 0.06	0.73 ± 0.09	0.67 ± 0.03*	0.75 ± 0.06
7	0.65 ± 0.08	0.46 ± 0.04*	0.44 ± 0.05*	0.41 ± 0.02*
14	0.44 ± 0.04	0.36 ± 0.01*	0.33 ± 0.02*	0.37 ± 0.03
21	0.41 ± 0.07	0.40 ± 0.06	0.36 ± 0.06	0.35 ± 0.06

* $P < 0.05$ vs control cements (0% ZnO).

Table 5

day	Cement 0% ZnO PO_4^{3-} (mM)	Cement 1% ZnO PO_4^{3-} (mM)	Cement 3% ZnO PO_4^{3-} (mM)	Cement 6% ZnO PO_4^{3-} (mM)
1	3.55 ± 0.44	3.44 ± 0.30	4.32 ± 0.13*	5.39 ± 0.35
3	1.23 ± 0.20	1.22 ± 0.13	1.21 ± 0.03	1.30 ± 0.05
7	0.77 ± 0.10	0.61 ± 0.06	0.58 ± 0.05*	0.56 ± 0.02*
14	0.53 ± 0.05	0.47 ± 0.02	0.43 ± 0.02*	0.48 ± 0.03
21	0.46 ± 0.07	0.44 ± 0.07	0.41 ± 0.07	0.41 ± 0.06

* $P < 0.05$ vs control cements (0% ZnO).

Table 6

Day	Cement 0% ZnO Zn^{2+} (mM)	Cement 1% ZnO Zn^{2+} (mM)	Cement 3% ZnO Zn^{2+} (mM)	Cement 6% ZnO Zn^{2+} (mM)
1	–	0.138 ± 0.013	0.769 ± 0.087	1.353 ± 0.071*
3	–	0	0.047 ± 0.002	0.171 ± 0.049
7	–	0	0	0.025 ± 0.005
14	–	0	0	0.004 ± 0.003
21	–	0	0	0

* $P < 0.05$ vs control cements (0% ZnO).

Table 7

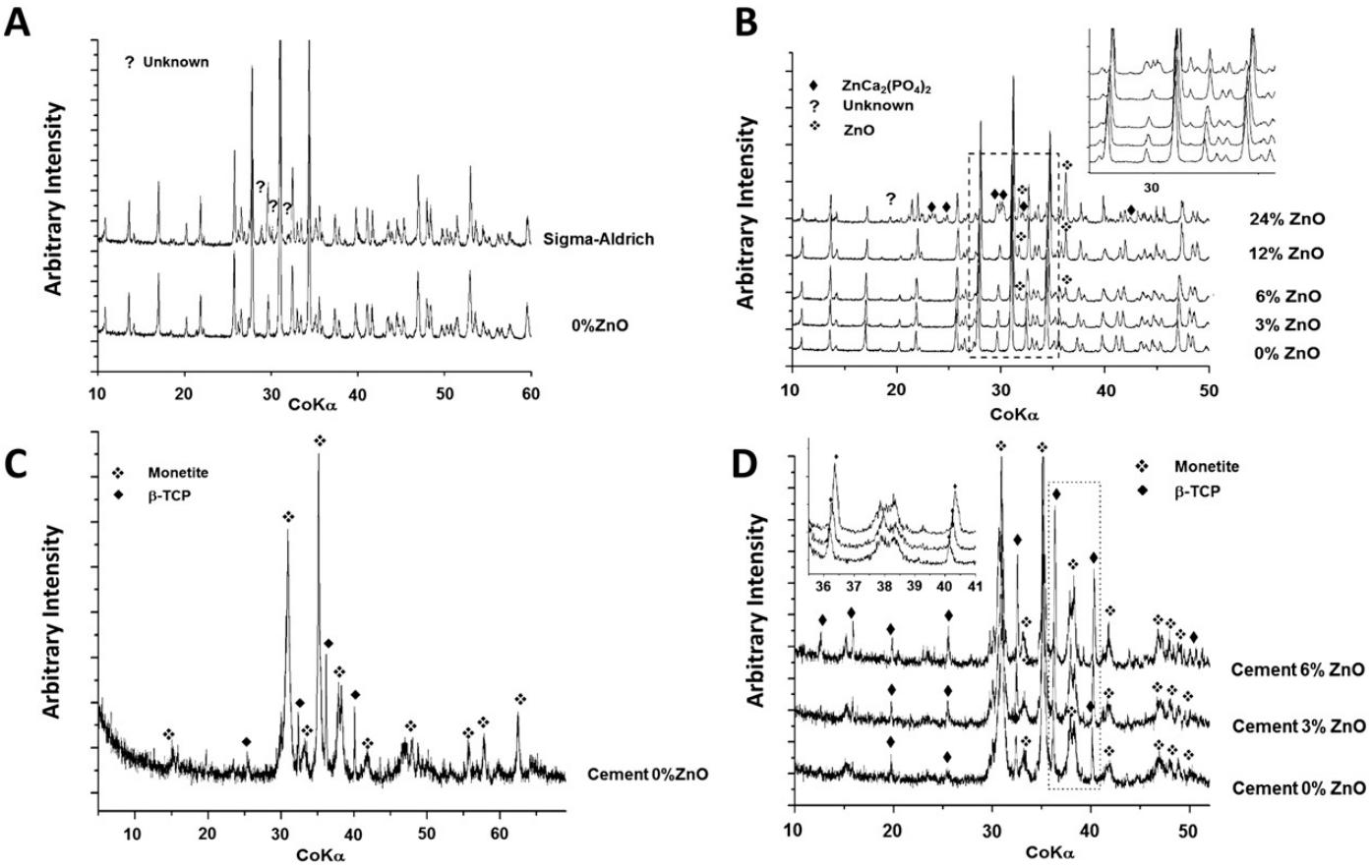

Figure 1

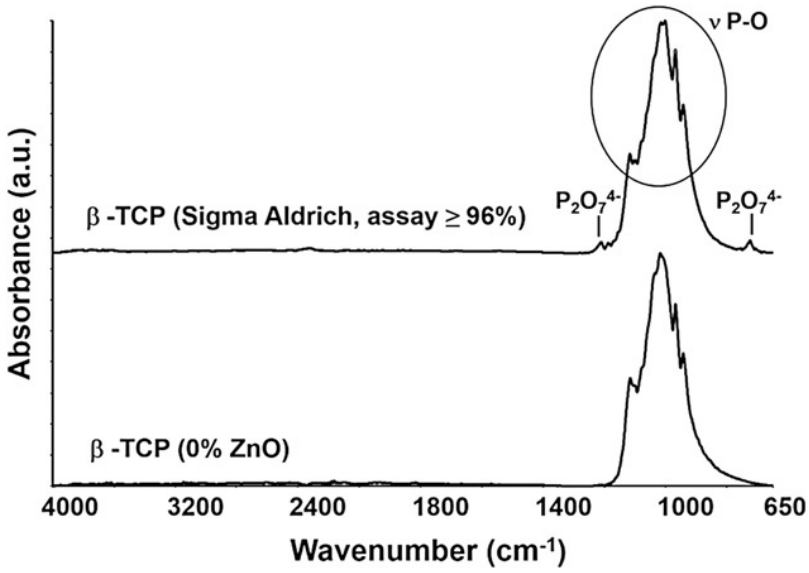

Figure 2

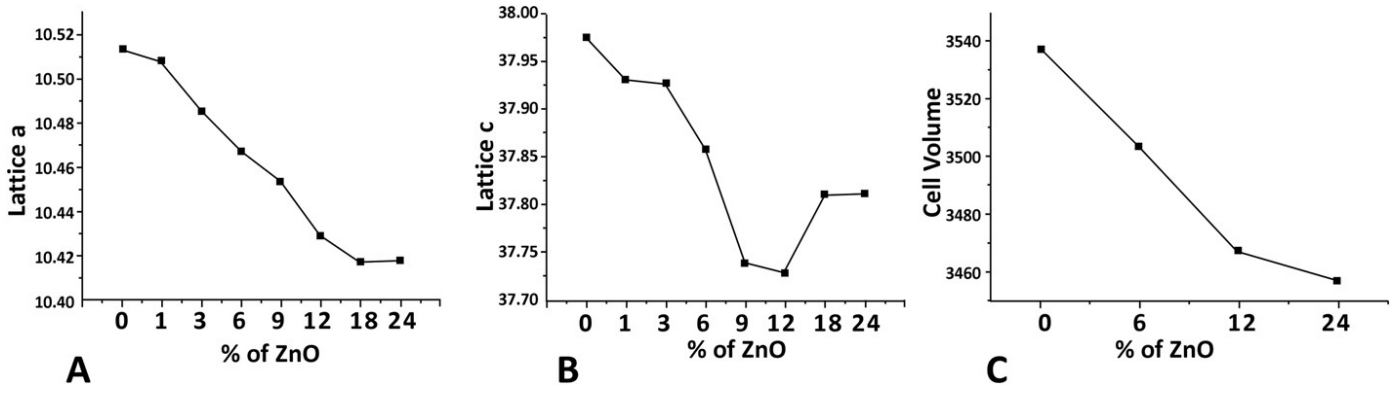

Figure 3

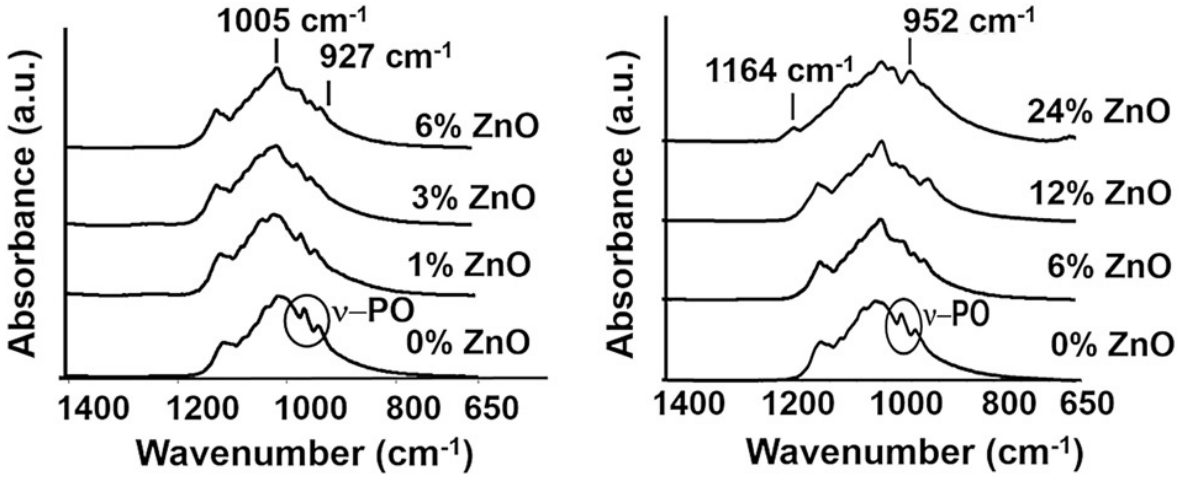

Figure 4

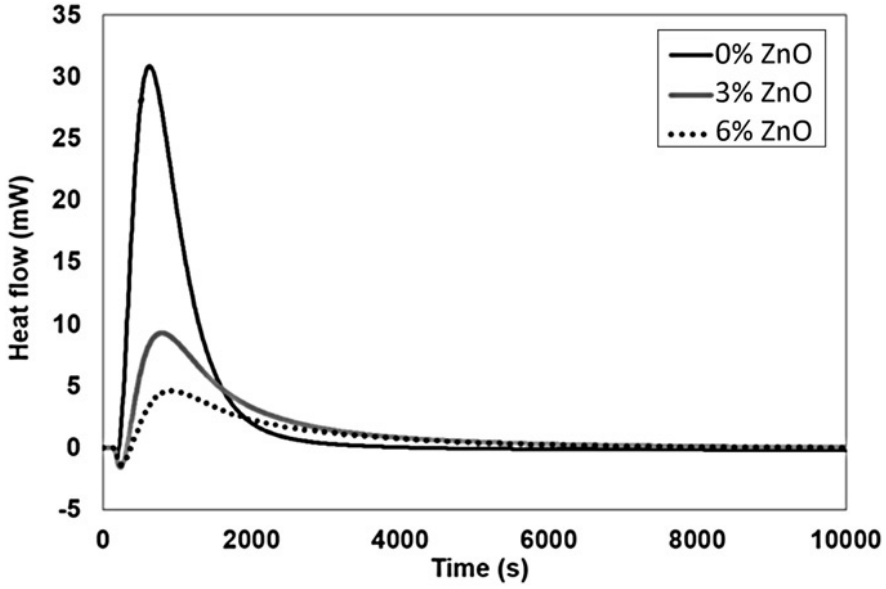

Figure 5

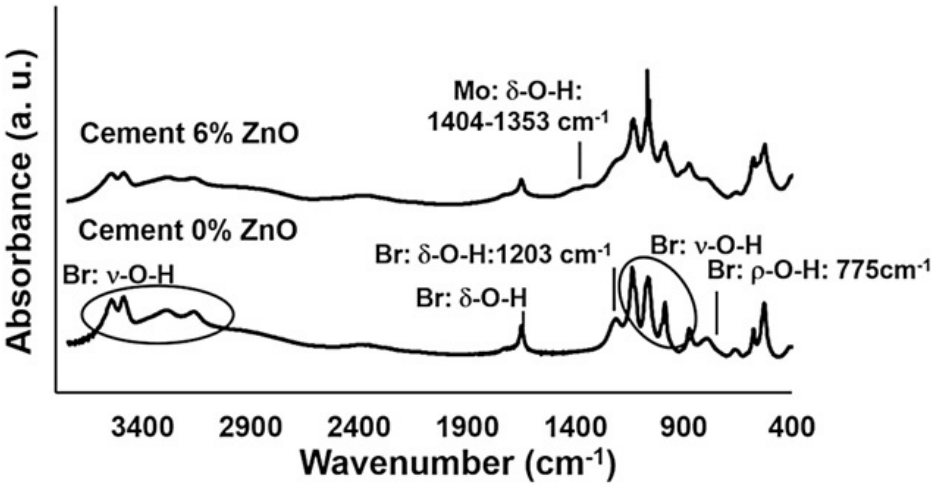
Absorbance (a. u.)
Cement 6% ZnO
Mo: δ-O-H:
1404-1353 cm-1
Cement 0% ZnO
Br: ν-O-H
Br: δ-O-H:1203 cm-1
Br: δ-O-H
Br: ν-O-H
Br: ρ-O-H: 775cm-1
3400
2900
2400
1900
1400
900
400
Wavenumber (cm-1)

Figure 6

Figure 7

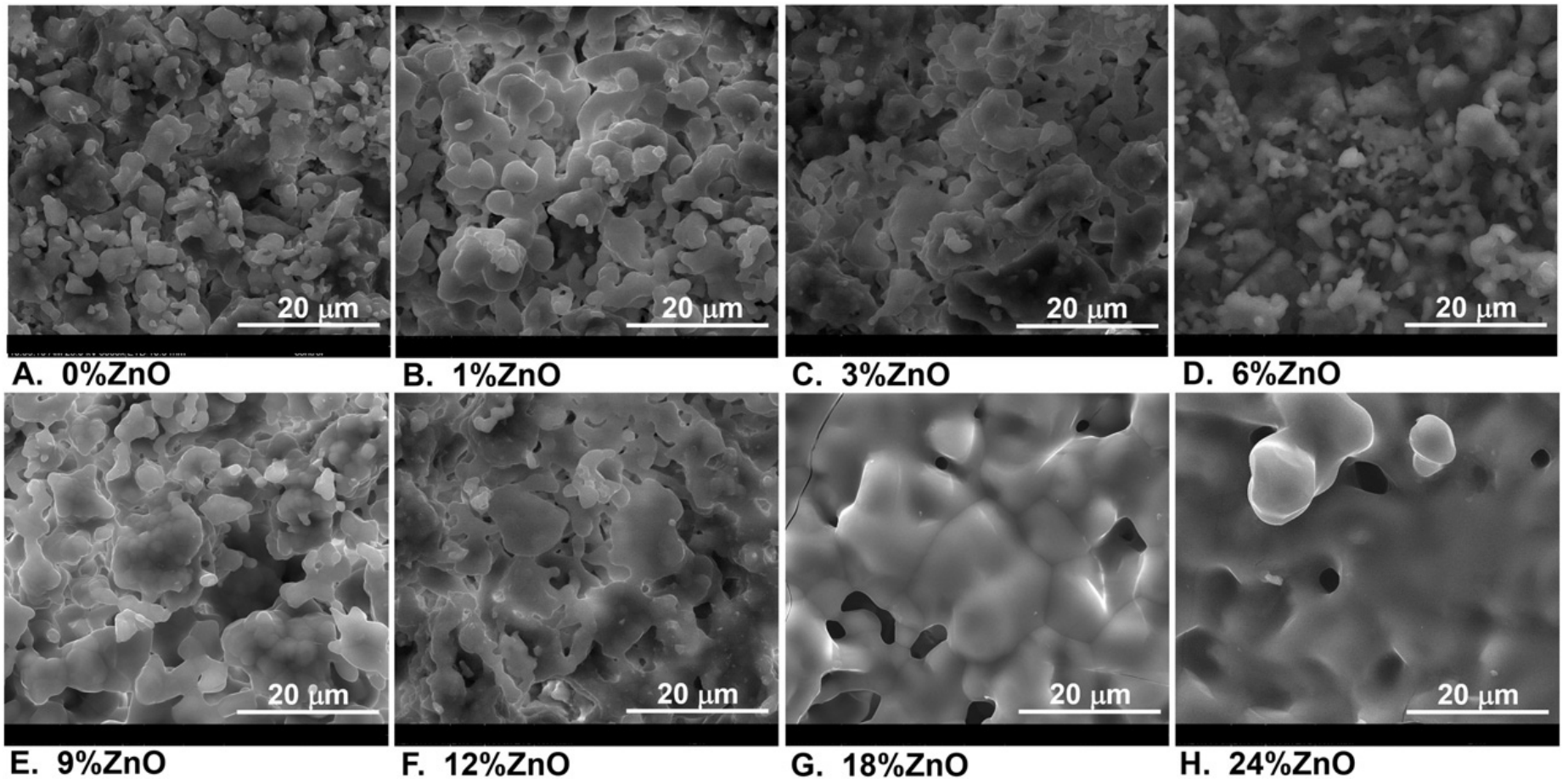
20 μm
A. 0%ZnO
20 μm
B. 1%ZnO
20 μm
C. 3%ZnO
20 μm
D. 6%ZnO
20 μm
E. 9%ZnO
20 μm
F. 12%ZnO
20 μm
G. 18%ZnO
20 μm
H. 24%ZnO

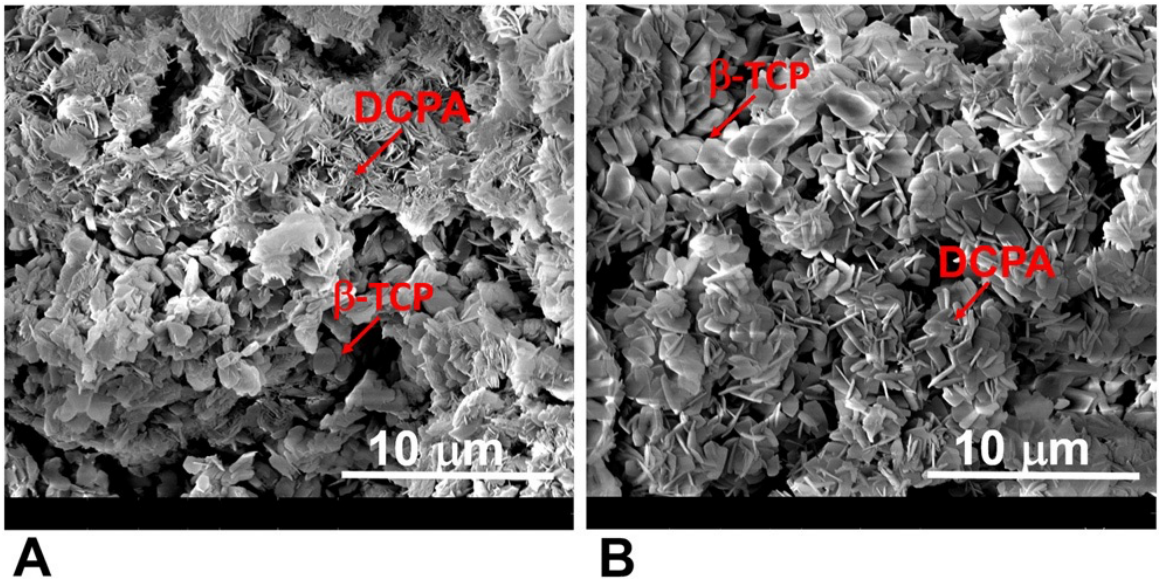

Figure 8

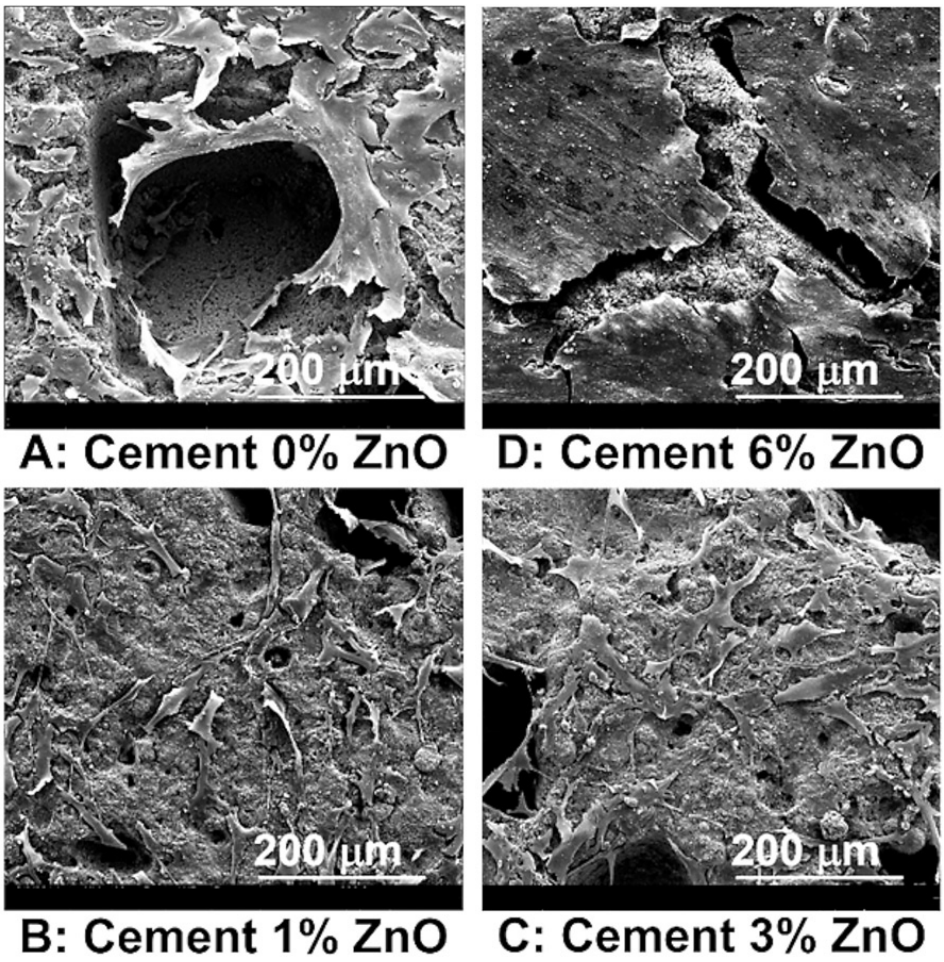

Figure 9

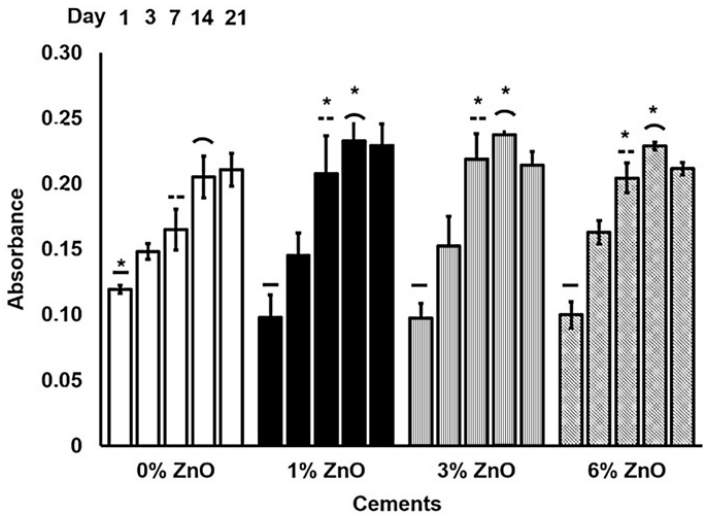
Day 1 3 7 14 21
0.30
0.25
0.20
0.15
0.10
0.05
0
Absorbance
0% ZnO
1% ZnO
3% ZnO
6% ZnO
Cements

Figure 10

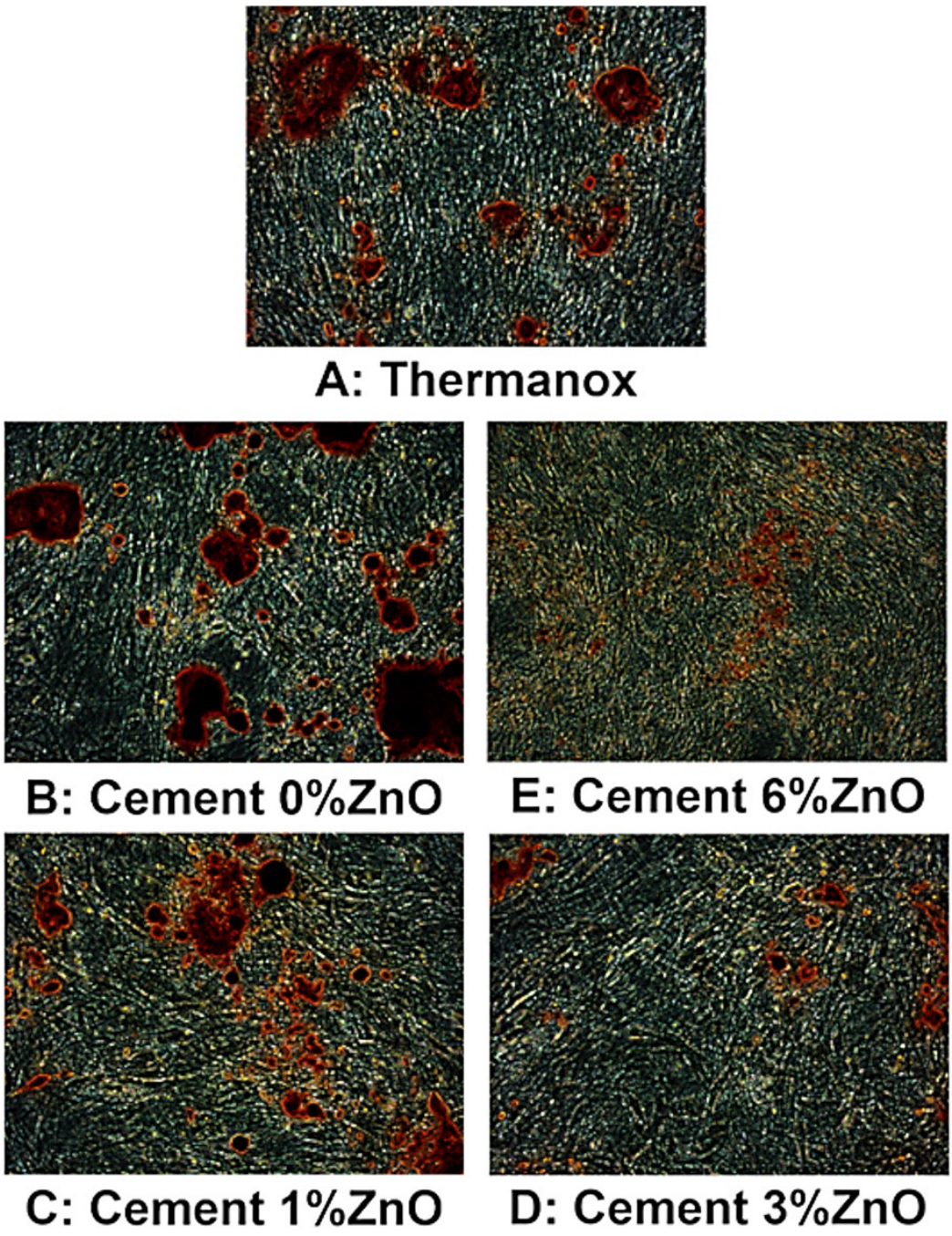
A: Thermanox
B: Cement 0%ZnO
E: Cement 6%ZnO
C: Cement 1%ZnO
D: Cement 3%ZnO

Figure 11

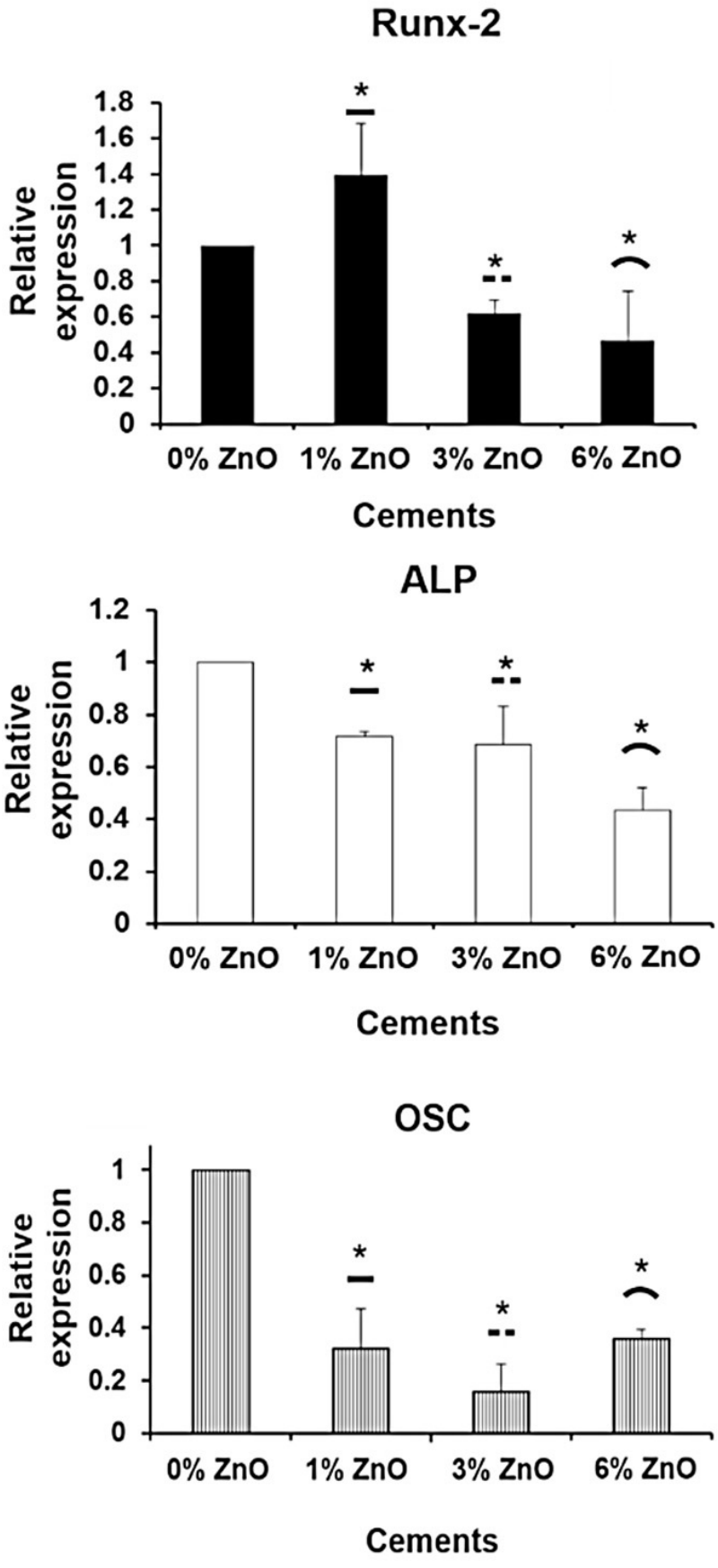
Runx-2
Relative expression
1.8
1.6
1.4
1.2
1
0.8
0.6
0.4
0.2
0
*
*
*
0% ZnO
1% ZnO
3% ZnO
6% ZnO
Cements
ALP
Relative expression
1.2
1
0.8
0.6
0.4
0.2
0
*
*
*
0% ZnO
1% ZnO
3% ZnO
6% ZnO
Cements
OSC
Relative expression
1
0.8
0.6
0.4
0.2
0
*
*
*
0% ZnO
1% ZnO
3% ZnO
6% ZnO
Cements

Figure 12